

Effect of doping on hot-carrier thermal breakdown in perforated graphene metasurfaces

M. Ryzhii^{1*}, V. Ryzhii^{2,3*}, C. Tang^{2,3}, T. Otsuji^{4,5,6}, and M. S. Shur^{7,8}

¹*School of Computer Science and Engineering, University of Aizu, Aizu-Wakamatsu 965-8580, Japan*

²*Research Institute of Electrical Communication, Tohoku University, Sendai 980-8577, Japan*

³*Frontier Research Institute for Interdisciplinary Sciences, Tohoku University, Sendai 980-8578, Japan*

⁴*International Research Institute of Disaster Science, Tohoku University, Sendai 980-8578, Japan*

⁵*Center of Excellence ENSEMBLE3, Warsaw 01-919, Poland*

⁶*UNIPRESS Institute of High Pressure Physics of the Polish Academy of Sciences, Warsaw 02-822, Poland*

⁷*Department of Electrical, Computer, and Systems Engineering, Rensselaer Polytechnic Institute, Troy, New York 12180, USA*

⁸*Electronics of the Future, Inc., Vienna, VA 22181-6117, USA*

*Authors to whom correspondence should be addressed: m-ryzhii@u-aizu.ac.jp, vryzhii@gmail.com

We examine the robustness of the S-shaped current–voltage characteristics associated with hot-carrier–induced electrical breakdown in perforated graphene metasurfaces (PGMs) as a function of doping. The perforation of the graphene layer forms interdigital arrays of graphene microribbons (GMRs) interconnected by graphene nanoribbon (GNR) bridges. These GNR constrictions act as energy barriers for electrons and holes emitted from the GMRs and govern the inter-GMR thermionic current under an applied bias voltage. The doping and the voltage bias establish distinct electron and hole populations in adjacent GMRs. Peltier heating of these carriers within the GMRs increases their effective temperatures, thereby enhancing the inter-GMR current. The resulting positive feedback between carrier heating and current amplification can trigger an electrothermal breakdown, transforming a superlinear current–voltage dependence into an S-shaped characteristic exhibiting negative differential resistance. The degree of electron–hole asymmetry significantly influences this positive feedback and strongly modifies the overall current–voltage response. These results provide a framework for optimizing PGM-based devices employing GMR/GNR architectures, including voltage-controlled fast switches, incandescent emitters, and terahertz bolometric detectors.

I. INTRODUCTION

The unique properties of graphene layers (GLs),^{1–4} in particular, patterned into graphene micro- and nanoribbons (GMRs and GNRs) and combined with two-dimensional van der Waals structures^{5–10} enable many device applications: terahertz and infrared detectors and sources, transistors and other devices.^{11–27} Recently, we demonstrated that perforated graphene layers, constituting arrays of coplanar interdigital graphene micro- and nanoribbons (GMRs and GNRs), can exhibit specific and pronounced plasmonic oscillations²⁸ and the hot-carrier thermal breakdown,^{29,30} which can be used in effective effective perforated graphene metasurfaces (PGMs) based terahertz photomixers and detectors^{31–33} and fast voltage-controlled switching devices.

The physical-mathematical model used in the previous analysis of similar PGMs assumed that the pristine GL and, hence, the GMRs fabricated via the perforation procedure, are undoped. Unintentional or intentional chemical GL doping can lead to a substantial non-equivalence of the oppositely polarized neighboring GMRs. As might be expected, this can result in different carrier densities and carrier emission from neighboring GMRs, as well as their effective temperatures. In this paper, we extend our previous analysis and device model,

providing a more comprehensive description of carrier transport and electrothermal feedback in doped PGM structures.

II. MAIN EQUATIONS OF THE PGM MODEL

Figure 1(a) presents the PGM based on the GMR/GNR structure created by the GL perforation. In the absence of the bias voltage, all the GMRs are filled with holes with the density close to acceptor density Σ_A (all the GMRs are of p-type). At sufficiently high bias voltages $V_G > V_A$, where $V_A \propto \Sigma_A$ is the doping (acceptor) voltage, the 2D electron and 2D hole systems are formed in the neighboring GMRs so that the n-GMRs and p-GMRs alternate. In the areas near the perforations, the n-GMRs and p-GMRs are separated by relatively high energy barriers for the electrons and holes. The heights of these barriers are determined by the band alignment between graphene and the substrate material, for example h-BN (although other substrate materials that provide a high-quality interface, such as SiC, can be used). In contrast, the GNRs offer relatively low energy barriers between the n-GMRs and p-GMRs. These barriers are associated with the lateral confinement of electron and hole motion in the GNRs (perpendicular to the GNRs) and the pertinent quantization of their energy spectra. Hence, the height of such barriers is deter-

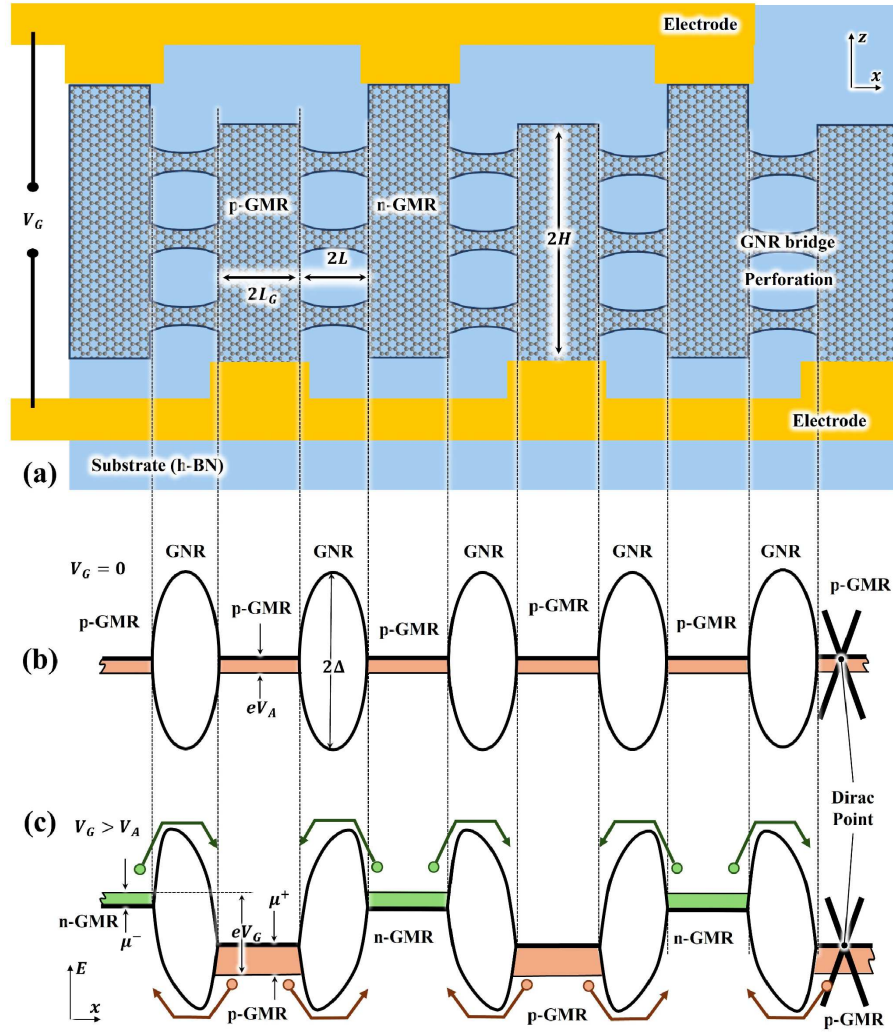


FIG. 1. (a) Top view of a PGM with metal contact electrodes, (b) its band diagram corresponding to cross-sections of the inter-GNR bridges at $V_G = 0$ and (c) at $V_G > V_A$.

mined by the GNR minimal thickness w . Figures 1(b) and 1(c) show the band diagrams without bias voltage and under a sufficiently high bias voltage $V_G > V_A$, respectively. The GMR ends are connected with the contact metal (or graphene) pads. The GMR/GNR structures under consideration are of $2H$ and $2L_G$ in the GMR length and width, respectively, with $(2N-1)$ of the GNRs bridging each GMR pair. The shape of the GL perforations is assumed to be relatively smooth (like an oval) so that the GNR barrier can be considered as approximately parabolic.

Using Landauer-Buttiker approach,³⁴ the thermionic current, j_{GMR} , through each GNR from one GMR to neighboring GMR can be presented as

$$j_{GNR} = j_{GNR}^- + j_{GNR}^+ \quad (1)$$

with

$$j_{GNR}^\mp \simeq \frac{4e}{\pi\hbar} \left[T^\mp \exp\left(\frac{\mu^\mp - \Delta + \eta eV_G}{T^\mp}\right) - T^\pm \exp\left(\frac{-\mu^\mp - \Delta - \eta eV_G}{T^\pm}\right) \right] \quad (2)$$

being the electron (marked by "-") and hole (marked by "+") components. Here, T^\pm are the electron and hole effective temperatures, $\mu^\mp \simeq \hbar v_W \sqrt{\pi \Sigma_G^\mp}$ are the Fermi energies in the pertinent GMRs with $\Sigma_G^\mp = C_G V_G / 2L_G e \mp \Sigma_A$ (for acceptor doping with the surface density Σ_A). The Fermi energies of the carriers induced in the GMRs by both acceptors and the bias voltage at not too low their densities can be presented as $\mu^\mp \simeq e \sqrt{V_G (V_G \mp V_A)}$, $V_A \simeq 2eL_G \Sigma_A / C_G$, $\bar{V}_G = (\pi C_G \hbar^2 v_W^2 / 2e^3 L_G)$ is the characteristic voltage, $c_G = [(\kappa_S + 1) / 4\pi^2] \bar{C}_G$ is the inter-GMR capacitance, which is determined by the geometrical parameters ratio L_G/L and the substrate dielectric constant κ_S ³⁵ (see as well Refs. 36 and 37),

v_W is the carrier velocity in GLs, and \hbar is the Planck constant. We assume that the GNR barrier is lowered by the voltage between the GMR so that the barrier is equal to $\Delta - \eta eV_G$, where η is determined by the shape of the GNR energy barrier. For near trapezoidal barriers $\eta \ll 1$, whereas for near-parabolic barriers with the top at the GNR center under consideration $\eta \simeq 1/2$. The latter is assumed in the following.

The second terms on the right sides of Eqs. (2), which are relatively small at sufficiently large V_G , correspond to the reverse thermionic currents - the electron current from the p-GMRs and the hole current from the n-GMRs. Equations (2) account for possible distinctions in the Fermi energies μ^- and μ^+ and in the effective temperatures T^- and T^+ in the n- and p-GMRs.

The electrons coming from the n-GMR into the p-GMR increase the energy of the holes and, therefore, heat the hole system in the latter, while the holes from the p-GMR heat the electron system in the n-GMR (the carrier heating due to the Peltier effect). Accounting for that the Joule heating associated with the currents along the GMRs can be weak if the conductance along them is high, we, disregarding the latter, use the following equations for the energy balance in the n- and p-GMRs:

$$2HC_G(V_G \mp V_A)R^\mp = (2N - 1)e j_{GMR}^\pm V_G. \quad (3)$$

This, in particular, implies a relatively small contribution of the quantum capacitance to the net inter-GMR capacitance and a smallness of the built-in voltage. According to the latter, we preserve the quantities μ^\mp in the exponents in Eqs. (2), disregarding them in other terms. The validity of Eqs. (3) is limited by the bias voltage range \bar{V}_G , $\mu^\mp \ll V_G, (V_G \mp V_A)$, in which one can expect the thermal breakdown effect explored below.

Considering the PGM structures at room temperature, we assume that the carrier energy relaxation is associated with optical phonons being the crucial mechanism (see, for example, Refs. 38 - 41). When the electron and hole systems are heated somewhat above room temperature, the rate of optical phonon relaxation can saturate. This is the main reason for the hot-carrier breakdown at a certain bias voltage V_G (at the threshold voltage V_G^{th}). In this case, other energy relaxation mechanisms can appear, determining the PGM structure characteristics beyond the threshold. For the sake of definiteness, we assume that such mechanisms are associated with the disordered-assisted electron-phonon scattering and the plasmon-assisted scattering.⁴²⁻⁴⁴ On the analogy with the previous studies (see, for example, Refs. 45 and 46), we set

$$R^\mp \simeq \frac{\hbar\omega_0}{\tau_{OP}} \left(\frac{T_0}{\hbar\omega_0} \right)^2 \left[\exp \left(\frac{\hbar\omega_0}{T_0} - \frac{\hbar\omega_0}{T^\mp} \right) - 1 + c \frac{(T^\mp)^3 - T_0^3}{T_0^3} \right]. \quad (4)$$

Here, $\tau_{OP} = \tau_0(T_0/\hbar\omega_0)^2 \exp(\hbar\omega_0/T_0)$ is the "warm" carrier energy relaxation time at T^\mp close to the lattice temperature T_0 , ω_0 and τ_0 are the optical phonon energy in GMRs

and the characteristic time of the spontaneous optical phonon emission, respectively, $c = (\tau_{OP}/\tau_{SC})(\hbar\omega_0/T_0)$ with τ_{SC} being the carrier energy relaxation time associated with the SC mechanism. When $T \simeq T_0$, Eqs. (4) transform to more standard form: $R^\mp \propto (T^\mp - T_0)$.

Equations (1) - (4) lead to the following equations parametrically relating j_{GMR}^\mp and V_G via T^\mp as parameters:

$$j_{GMR}^\mp \simeq j_N \frac{V_G \mp V_A}{V_G} \left[\exp \left(\frac{\hbar\omega_0}{T_0} - \frac{\hbar\omega_0}{T^\mp} \right) - 1 + c \frac{(T^\mp)^3 - T_0^3}{T_0^3} \right] \quad (5)$$

and

$$j_{GMR}^\mp = j_T \left\{ \frac{T^\mp}{T_0} \exp \left[\frac{e\sqrt{V_G(V_G \mp V_A)} + eV_G/2 - \Delta}{T^\mp} \right] - \frac{T^\pm}{T_0} \exp \left[\frac{e\sqrt{V_G(V_G \mp V_A)} - eV_G/2 - \Delta}{T^\pm} \right] \right\}. \quad (6)$$

Combining Eqs. (5) and (6), we arrive at the following equation, which relates the carrier temperatures T^- and T^+ in the n-GNRs and p-GNRs and the bias voltages V_G :

$$\begin{aligned} \beta_N \frac{(V_G \mp V_A)}{V_G} \left[\exp \left(\frac{\hbar\omega_0}{T_0} - \frac{\hbar\omega_0}{T^\mp} \right) - 1 + c \frac{(T^\mp)^3 - T_0^3}{T_0^3} \right] \\ = \frac{T^\pm}{T_0} \exp \left[\frac{e\sqrt{V_G(V_G \pm V_A)} + eV_G/2 - \Delta}{T^\pm} \right] \\ - \frac{T^\mp}{T_0} \exp \left[\frac{e\sqrt{V_G(V_G \pm V_A)} - eV_G/2 - \Delta}{T^\mp} \right], \end{aligned} \quad (7)$$

where $\beta_N = [\pi HC_G \hbar / 2(2N - 1)e^2 \tau_0^\varepsilon](T_0/\hbar\omega_0)$. If $H = 1.0 \mu\text{m}$, $C_G = 1$, and $\tau_{OP} = 20 \text{ ps}$, $\beta_N \simeq 4.268 \times 10^{-3} / (2N - 1)$.

If $V_A = 0$, $T^\mp = T$ and Eqs. (7) yield

$$\begin{aligned} \frac{\beta_N}{2} \left[\exp \left(\frac{\hbar\omega_0}{T_0} - \frac{\hbar\omega_0}{T} \right) - 1 + c \frac{T^3 - T_0^3}{T_0^3} \right] \\ = \frac{T}{T_0} \exp \left(\frac{e\sqrt{V_G V_G} - \Delta}{T} \right) \sinh \left(\frac{eV_G}{2T} \right). \end{aligned} \quad (8)$$

Equation (8) leads to the $T - V_G$ characteristics, which can exhibit the thermal breakdown provided sufficiently small values of β_N [or large number of the GNR bridges $(2N - 1)$] predicted previously.²⁸

The net terminal current in the PGM with M GMR pairs is equal to

$$J_{GMR} = M(2N - 1)(j_{GMR}^- + j_{GMR}^+). \quad (9)$$

H , nm	L , nm	L_G , nm	w , nm	Δ , meV	κ_S	C_G	V_G , mW	T_0 , meV	$\hbar\omega_0$, meV	τ_{OP} , ps	τ_{SC} , ps	β_1
1000	25	25	10	250	10	1	8	25	200	20	160	4.27×10^{-3}

TABLE I. Main PGM parameters

III. RESULTS: VOLTAGE DEPENDENCES OF CARRIER EFFECTIVE TEMPERATURES AND CURRENT-VOLTAGE CHARACTERISTICS

For the illustration, we solved the system of coupled Eqs. (7) numerically using MATLAB (R2024b). Since the pair of implicit Eqs. (7) with multiple solutions for T can not be solved directly by the exchange of variables, we utilized MATLAB built-in function *vpasolve*, calculating parts of the curves of the system below and above (on the temperature axis) the threshold points separately, guessing their initial value ranges. The main PGM parameters used for the calculations are listed in Table I and include a different number, $(2N - 1)$, of GNR bridges connecting the GMRs and different donor voltages V_A in the range $V_G > V_A$. The calculation results are presented in Figs. 2–4.

Figure 2(a) shows that in the undoped PGMs ($V_A = 0$),

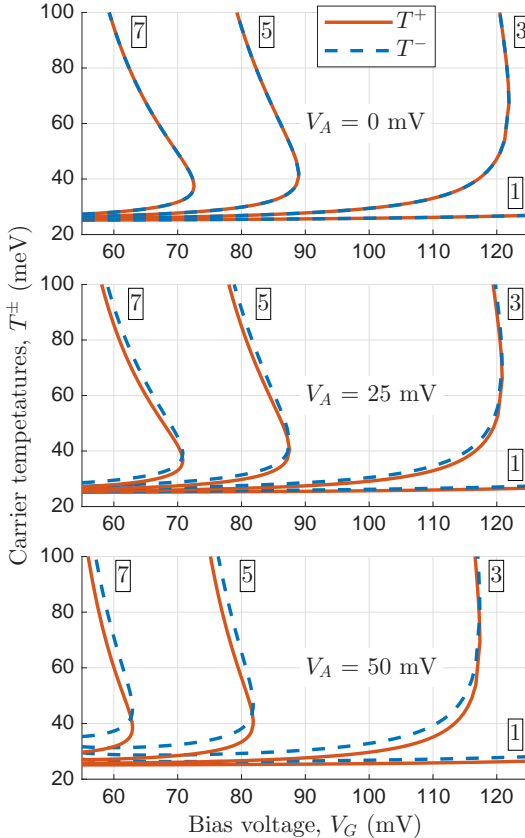


FIG. 2. Voltage dependences of carrier temperatures T^- and T^+ in the PGMs with different numbers, $(2N - 1) = 1, 3, 5, 7$ of the GNR bridges (indicated in rectangles) and different doping voltages: $V_A = 0$ ($T^- = T^+ = T$), $V_A = 25$ mV, and $V_A = 50$ mV (acceptor surface densities $\Sigma_A = 0$, $\Sigma_A \simeq 3.47 \times 10^{11}$ cm 2 , and $\Sigma_A \simeq 6.94 \times 10^{11}$ cm 2).

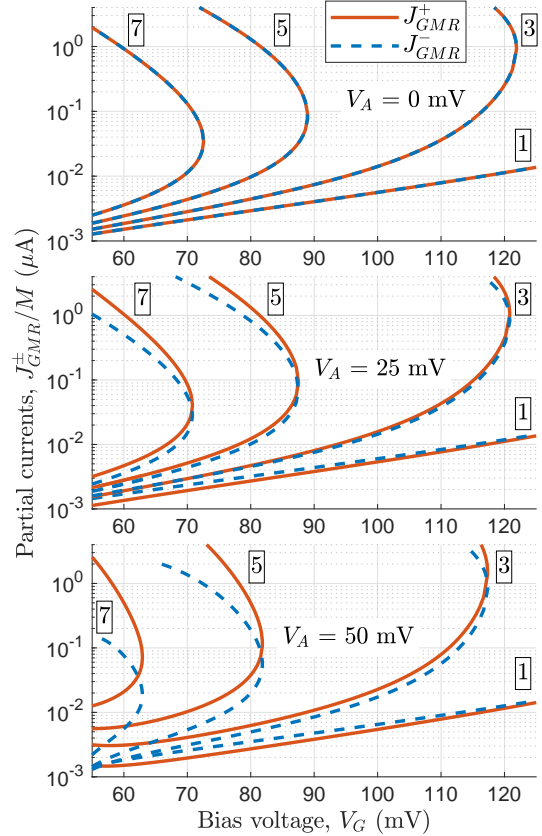


FIG. 3. Voltage dependences of partial currents of J_{GMR}^-/M and J_{GMR}^+/M normalized by the number, M , of the GMR pairs in the PGMs with different numbers, $(2N - 1)$, of the GNR bridges and different doping voltages V_A .

the carrier temperatures in the neighboring GMRs are equal ($T^- = T^+ = T$ being transformed from monotonous (rising, sublinear) and ambiguous functions of the bias voltage V_G depending on the number of the GNR bridges $(2N - 1)$). This transformation is due to the reinforcement of the injection between the GMRs with an increasing number of injecting channels, i.e., the number of the GNR bridges. The latter results in a stronger carrier overheating. We refer to such a characteristic transformation as hot-carrier thermal breakdown. It is attributed to positive feedback between the carrier heating and carrier injection between neighboring GMRs. The ambiguous dependences are characterized by the threshold voltage V_G^{th} , at which the derivative dT/dV_G escapes to infinity. Apart from two branches of the $T - V_G$ shown in Fig. 2, the ambiguous characteristics corresponding to a sufficiently large $(2N - 1)$ exhibit the appearance of the third, high-temperature branch with $dT/dV_G > 0$. These $T - V_G$ relations for these branches are determined by the high-temperature mechanisms of car-

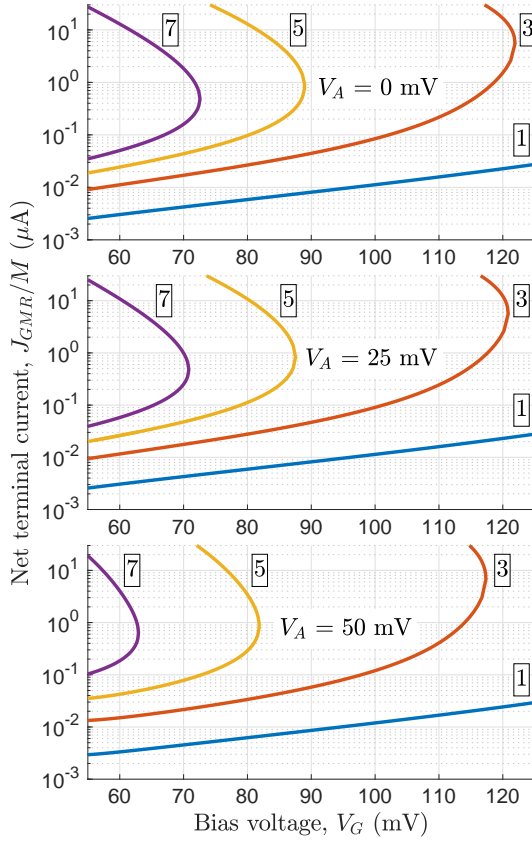


FIG. 4. Normalized current-voltage characteristics J_{GMR}/M of the PGMs with different $(2N - 1)$ and V_A .

rier relaxation (focusing on the doping effects, we do not consider the high-temperature branch here, see Ref. 29). Hence, at large $(2N - 1)$, the $T - V_G$ relations have an S-shape.

As seen in Fig. 2 for doped PGMs (middle and lower panels), the doping leads to a splitting of the $T^- - V_G$ and $T^+ - V_G$ voltage dependences associated with the non-equivalence (violation of the symmetry) of the n- and p-GMRs. Comparing the panels in Fig. 2, one sees that this splitting increases with increasing doping level (increasing doping voltage V_A) with the electron temperature T^- somewhat exceeding the hole temperature T^+ . This is because the electron density is smaller than that of the holes (if $V_A > 0$), while the hole current injected into the n-GMR is larger than the electron current injected into the p-GMRs (see Fig. 3 below). Nevertheless, both the $T^- - V_G$ and $T^+ - V_G$ relations are characterized by the same threshold voltage V_G^{th} .

Figure 3 shows that the doping affects the voltage dependences of the partial currents $J_{GMR}^-/M = (2N - 1)jGMR^-$ and $J_{GMR}^+/M = (2N - 1)jGMR^+$ (per one GMR pair), also resulting in their splitting, although the type of these characteristics is preserved (at least at the doping levels under consideration). Stronger variations of the $J_{GMR}^- - V_G$ and $J_{GMR}^+ - V_G$ characteristics compared to the $T^- - V_G$ and $T^+ - V_G$ relations are attributed to an exponential dependence of the partial currents on the carrier temperatures T^- and T^+ and the carrier Fermi energies μ^- and μ^+ . The $T^- - V_G$ and $T^+ - V_G$ relations on

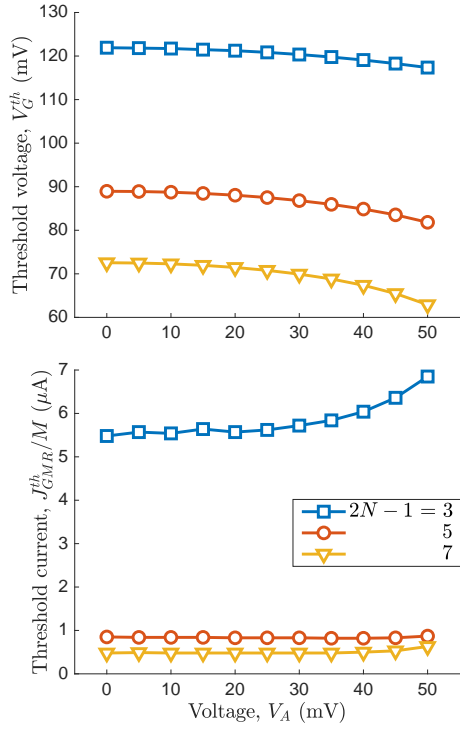


FIG. 5. Threshold voltage V_G^{th} (top panel) and threshold normalized current J_{GMR}^{th} (bottom panel) as functions of the doping voltage V_A for the PGMs with different $(2N - 1)$.

the one hand and the $J_{GMR}^- - V_G$ and $J_{GMR}^+ - V_G$ characteristics on the other correspond to the same values of the threshold voltage V_G^{th} . The latter is because when $dT^\pm/dV_G \Rightarrow \infty$ at V_G tending to V_G^{th} , $dJ_{GMR}^\pm/dV_G \Rightarrow \infty$, due to proportionality of dJ_{GMR}^\pm/dV_G to dT^\pm/dV_G .

Although the splitting of the $T^- - V_G$ and $T^+ - V_G$ characteristics with increasing doping voltage appears to be moderate, the doping affects the $J_{GMR}^- - V_G$ and $J_{GMR}^+ - V_G$ characteristics much more pronouncedly.

As seen in Fig. 4, the net current-voltage characteristics $J_{GMR} - V_G$ (normalized by the number, M , of GMR pairs) qualitatively repeat the behavior of the partial currents, being also sensitive to the doping level and, particularly, to the number of the GNR bridges $(2N - 1)$.

Figure 5 shows the noticeable (but not critical) variations in the threshold voltage and normalized threshold current, V_G^{th} and J_{GMR}^{th}/M , with increasing doping voltage V_A . At the same time, as can be seen from Fig. 5 (and Fig. 4), the former are very sensitive to the number of the GNR bridges $(2N - 1)$.

IV. CONCLUSIONS

We have shown that: (1) depending on the PGM structural parameters, the carrier temperature-voltage in the PGMs and their current-voltage characteristics can be fairly steep, being monotonous or ambiguous and tending to a S-shape - the effect of hot-carrier breakdown; (2) these dependences are

modified with increasing doping level; (3) the effect of hot-carrier breakdown is preserved up to rather high doping levels in the PGMs, being fairly sensitive to the number of the GNR bridges connecting the neighboring GMRs.

The obtained results can be used for the realization of novel PGM-based devices, such as fast voltage-controlled switches of the current, thermal incandescent light sources, and terahertz bolometers and their optimization.

ACKNOWLEDGMENTS

The work at Research Institute of Electrical Communication (RIEC), Frontier Institute for Interdisciplinary Studies (FRIIS), and University of Aizu (UoA) was supported by the Japan Society for the Promotion of Science (KAKENHI Grants Nos. 25K01281 and 25K22093), The Telecommunications Advancement Foundation, SCAT, JST ALCA-Next, and NEDO, Japan. The work at ENSEMBLE3 Ltd. was supported under the International Research Agenda program of the Foundation for Polish Science (FENG.02.01-IP.05-0044/24), the European Union through the Horizon 2020 Teaming for Excellence program (GA No. 857543), and the Poland Minister of Science and Higher Education Center of Excellence project under the Horizon 2020 program (No. MEiN/2023/DIR/3797).

DATA AVAILABILITY

All data that support the findings of this study are available within the article.

- ¹A. H. Castro Neto, F. Guinea, N. M. R. Peres, K. S. Novoselov, and A. K. Geim, “The electronic properties of graphene,” *Rev. Mod. Phys.* **81**, 109 (2009).
- ²A. S. Mayorov, R. V. Gorbachev, S. V. Morozov, L. Britnell, R. Jalil, L. A. Ponomarenko, P. Blake, K. S. Novoselov, K. Watanabe, T. Taniguchi, and A. K. Geim, “Micrometer-scale ballistic transport in encapsulated graphene at room temperature,” *Nano Lett.* **11**, 2396 (2011).
- ³D. G. Purdie, N. M. Pugno, T. Taniguchi, K. Watanabe, A. C. Ferrari, and A. Lombardo, “Cleaning interfaces in layered materials heterostructures,” *Nat. Comm.* **9**, 5387 (2018).
- ⁴D. De Fazio, D. G. Purdie, A. K. Ott, P. Braeuninger-Weimer, T. Khodkov, S. Goossens, T. Taniguchi, K. Watanabe, P. Livreri, F. H. L. Koppens, S. Hofmann, I. Goykhman, A. C. Ferrari, and A. Lombardo, “High-mobility, wet-transferred graphene grown by chemical vapor deposition,” *ACS Nano* **13**, 8926 (2019).
- ⁵M. Yankowitz, Q. Ma, P. Jarillo-Herrero, and B. J. LeRoy, “Van der Waals heterostructures combining graphene and hexagonal boron nitride,” *Nat. Rev. Phys.* **1**, 112 (2019).
- ⁶M. Y. Han and P. Kim, “Graphene nanoribbon devices at high bias,” *Nano Convergence* **1**, 1 (2014).
- ⁷Z. Chen, A. Narita, and K. Müllen, “Graphene nanoribbons: On-surface synthesis and integration into electronic devices,” *Adv. Mat.* **32**, 2001893 (2020).
- ⁸Y. Zhai, Y. Xiang, W. Yuan, G. Chen, J. Shi, G. Liang, Z. Wen, and Y. Wu, “Fabrication of graphene nanomesh FET terahertz detector,” *Micro-machines (Basel)* **12**, 641 (2021).
- ⁹Yi Lin, Y. Liao, Z. Chen, and J. W. Connell, “Holey graphene: a unique structural derivative of graphene,” *Mat. Res. Lett.* **5**, 209 (2017).
- ¹⁰P. Dubček, D. Ivezović, T. Čižmar, and M. Karlušić, “Nanoscale perforation of graphene by grazing-incidence swift heavy-ion irradiation,” *J. Phys. D: Appl. Phys.* **58**, 195304 (2025).
- ¹¹V. Ryzhii, M. Ryzhii, and T. Otsuji, “Negative dynamic conductivity of graphene with optical pumping,” *J. Appl. Phys.* **101**, 083114 (2007).

- ¹²V. Ryzhii, M. Ryzhii, V. Mitin, and T. Otsuji, “Toward the creation of terahertz graphene injection laser,” *J. Appl. Phys.* **110**, 094503 (2013).
- ¹³V. Ryzhii, M. Ryzhii, V. Mitin, M. S. Shur, A. Satou, and T. Otsuji, “Terahertz photomixing using plasma resonances in double-graphene layer structures,” *J. Appl. Phys.* **113**, 174506 (2013).
- ¹⁴V. Ryzhii, M. Ryzhii, M. S. Shur, V. Mitin, A. Satou, and T. Otsuji, “Resonant plasmonic terahertz detection in graphene split-gate field-effect transistors with lateral p-n junctions,” *J. Phys. D: Appl. Phys.* **49**, 315103 (2016).
- ¹⁵Y. Koseki, V. Ryzhii, T. Otsuji, V. V. Popov, and A. Satou, “Giant plasmon instability in a dual-grating-gate graphene field-effect transistor,” *Physical Review B* **93**, 245408 (2016).
- ¹⁶A. Rogalski, “Graphene-based materials in the infrared and terahertz detector families: a tutorial,” *Advances in Optics and Photonics*, **11**, 314 (2019).
- ¹⁷J. Liu, X. Li, R. Jiang, K. Yang, J. Zhao, S. A. Khan, J. He, P. Liu, J. Zhu, and B. Zeng, “Recent progress in the development of graphene detector for terahertz detection,” *Sensors (Basel)*, **21**, 4987 (2021).
- ¹⁸S. Boubanga-Tombet, W. Knap, D. Yadav, A. Satou, D. B. But, V. V. Popov, I. V. Gorbenko, V. Kachorovskii, and T. Otsuji, “Room temperature amplification of terahertz radiation by grating-gate graphene structures,” *Phys. Rev. X* **10**, 031004 (2020).
- ¹⁹T. Otsuji, S. A. Boubanga-Tombet, A. Satou, D. Yadav, H. Fukidome, T. Watanabe, T. Suemitsu, A. A. Dubinov, V. V. Popov, W. Knap, V. Kachorovskii, K. Narahara, M. Ryzhii, V. Mitin, M. S. Shur, and V. Ryzhii, “Graphene-based plasmonic metamaterial for terahertz laser transistors,” *Nanophotonics* **11**, 1677 (2022).
- ²⁰K. Tamura, C. Tang, D. Ogiura, et al. “Fast and sensitive terahertz detection with an epitaxial graphene asymmetric dual-grating-gate field- effect transistor structure,” *APL Photonics*, **7**, 126101 (2022).
- ²¹V. Ryzhii, T. Otsuji, M. Ryzhii, A. A. Dubinov, V. Ya. Aleshkin, V. E. Karasik, and M. S. Shur, “Negative terahertz conductivity and amplification of surface plasmons in graphene–black phosphorus injection laser heterostructures,” *Phys. Rev. B* **100**, 115436 (2019).
- ²²J. A. Delgado-Notario, W. Knap, V. Clericò, J. Salvador-Sánchez, J. Calvo-Gallego, T. Taniguchi, K. Watanabe, T. Otsuji, V. V. Popov, D. V. Fateev, E. Diez, J. E. Velázquez-Pérez, and Y. M. Meziani, “Enhanced terahertz detection of multigate graphene nanostructures,” *Nanophotonics* **11**, 519 (2022).
- ²³V. Ryzhii, C. Tang, T. Otsuji, M. Ryzhii, V. Mitin, and M. S. Shur, “Effect of electron thermal conductivity on resonant plasmonic detection in the metal/black-AsP/graphene FET terahertz hot-electron bolometers,” *Phys. Rev. Appl.* **19**, 064033 (2023).
- ²⁴V. Ryzhii, C. Tang, T. Otsuji, M. Ryzhii, V. Mitin, and M. S. Shur, “Dynamic characteristics of terahertz hot-electron graphene FET bolometers: Effect of electron cooling in channel and at side contacts,” *J. Appl. Phys.* **135**, 194502 (2024).
- ²⁵Y. Wei, Z. Bao, H. Wu, Y. Zhang, Y. Wen, Z. Hu, X. Pan, S. Lan, L. Zhang, L. Wang, and X. Chen, “High-performance terahertz photodetection in 2D materials and topological materials,” *J. Phys. D: Appl. Phys.* **58**, 073002 (2024).
- ²⁶A. J. Jumaah, H. G. Roskos, and S. Al-Daffaie, “Novel antenna-coupled terahertz photodetector with graphene nanoelectrodes,” *APL Photon.* **8**, 026103 (2023).
- ²⁷J. M. Caridad, O. Castello, S. M. Lopez Baptista, T. Taniguchi, K. Watanabe, H. G. Roskos, and J. A. Delgado-Notario, “Room-temperature plasmon-assisted resonant THz detection in single-layer graphene transistors,” *Nano Lett.* **24**, 935 (2024).
- ²⁸V. Ryzhii, C. Tang, T. Otsuji, M. Ryzhii, and M. S. Shur, “Terahertz plasmonic resonances in coplanar graphene nanoribbon structures,” *J. Appl. Phys.* **135**, 114503 (2024).
- ²⁹V. Ryzhii, C. Tang, M. Ryzhii, and M. S. Shur, “Hot-carrier thermal breakdown and S-type current–voltage characteristics in perforated graphene structures,” *AIP Advances* **15**, 075204 (2025).
- ³⁰V. Ryzhii, M. Ryzhii, S. Shur, T. Otsuji, and C. Tang, “Thermal hot-carrier breakdown in metasurface structures based on coplanar arrays of graphene microribbons connected with wide-gap bridges,” *arXiv:2511.03975v1* (2025).
- ³¹V. Ryzhii, M. Ryzhii, C. Tang, T. Otsuji, and M. S. Shur, “Resonant plasmonic terahertz photomixing using interdigital graphene micro-nanoribbon arrays,” *Appl. Phys. Lett.* **124**, 163504 (2024).

³²V. Ryzhii, C. Tang, T. Otsuji, M. Ryzhii, and M. S. Shur, "Detection of terahertz radiation using topological graphene micro- nanoribbon structures with transverse plasmonic resonant cavities," *J. Appl. Phys.* **136**, 194502 (2024).

³³V. Ryzhii, C. Tang, M. Ryzhii, T. Otsuji, and M. S. Shur, "Rectification and bolometric terahertz radiation detectors based on perforated graphene structures exhibiting plasmonic resonant response," *J. Appl. Phys.* **137**, 244501 (2025).

³⁴M. Buttiker, Y. Imry, R. Landauer, and S. Pinhas, "Generalized many-channel conductance formula with application to small rings," *Phys. Rev. B* **3**, 6207 (1985).

³⁵A. Sh. Achoyan, A. E. Yesayan, E. M. Kazaryan, S. G. Petrosyan, "Two-dimensional p-n junction under equilibrium conditions," *Semiconductors* **36**, 903 (2002).

³⁶B. Gelmont, M. Shur, and C. Moglestue, "Theory of junction between two-dimensional electron gas and p-type semiconductor," *IEEE Trans. Electron Devices* **39**, 1216 (1992).

³⁷O. G. Vendik, S. P. Zubko, M. A. Nikol'skii, "Modeling and calculation of the capacitance of a planar capacitor containing a ferroelectric thin film," *Tech. Phys.* **44**, 349 (1999).

³⁸H. Wang, J. H. Strait, P. A. George, S. Shivaraman, V. D. Shields, M. Chandrashekhar, J. Hwang, F. Rana, M. G. Spencer, C. S. Ruiz-Vargas, and J. Park, "Ultrafast relaxation dynamics of hot optical phonons in graphene," *Appl. Phys. Lett.* **96**, 081917 (2010).

³⁹K. M. Borysenko, J. T. Mullen, E. A. Barry, S. Paul, Y. G. Semenov, J. M. Zavada, M. Buongiorno Nardelli, and K.W. Kim, "First-principles analysis of electron-phonon interactions in graphene," *Phys. Rev. B* **81**, 121412R (2010).

⁴⁰M. V Fischetti, D. K. Ferry, and S. J. Aboud, "Pseudopotential-based studies of electron transport in graphene and graphene nanoribbons," *J. Phys: Cond. Mat.* **25**, 473202 (2013).

⁴¹E. A. A. Pogna, X. Jia, A. Principi, A. Block, L. Banszerus, J. Zhang, X. Liu, T. Sohier, S. Forti, K. Soundarapandian, B. Terrés, J. D. Mehew, C. Trovatello, C. Coletti, F. H. L. Koppens, M. Bonn, H. I. Wang, N. van Hulst, M. J. Verstraete, H. Peng, Z. Liu, C. Stampfer, G. Cerullo, and K.-J. Tielrooij, "Hot-carrier cooling in high-quality graphene is intrinsically limited by optical phonons," *ACS Nano* **15**, 11295 (2021).

⁴²J. C. W. Song, M. Y. Reizer, and L. S. Levitov, "Disorder-assisted electronphonon scattering and cooling pathways in graphene," *Phys. Rev. Lett.* **109**, 106602 (2012).

⁴³D. K. Ferry, H. Ramamoorthy, and J. P. Bird, "Plasmon-mediated energy relaxation in graphene," *Appl. Phys. Lett.* **107**, 262103 (2015).

⁴⁴D. K. Ferry, R. Somphonsane, H. Ramamoorthy, and J. P. Bird, "Energy relaxation of hot carriers in graphene via plasmon interaction," *J. Comput. Electron.* **15**, 144 (2016).

⁴⁵V. Ryzhii, M. Ryzhii, V. Mitin, A. Satou, and T. Otsuji, "Effect of heating and cooling of photogenerated electron-hole plasma in optically pumped graphene on population inversion," *Jpn. J. Appl. Phys.* **50**, 094001 (2011).

⁴⁶V. Ryzhii, T. Otsuji, M. Ryzhii, N. Ryabova, S. O. Yurchenko, V. Mitin, and M. S. Shur, "Graphene terahertz uncooled bolometers," *J. Phys. D: Appl. Phys.* **46**, 065102 (2013).